


Article

Intercalation and Exfoliation of Kaolinite with Sodium Dodecyl Sulfate

Xiaochao Zuo ^{1,2}, Ding Wang ³, Shilong Zhang ³, Qinfu Liu ^{3,*} and Huaming Yang ^{1,2,*} 

¹ Centre for Mineral Materials, School of Minerals Processing and Bioengineering, Central South University, Changsha 410083, China; xiaochaozuo@csu.edu.cn

² Hunan Key Lab of Mineral Materials and Application, Central South University, Changsha 410083, China

³ School of Geoscience and Surveying Engineering, China University of Mining & Technology, Beijing 100083, China; wangding0313@163.com (D.W.); cailiao007@163.com (S.Z.)

* Correspondence: lqf@cumt.edu.cn (Q.L.); hmyang@csu.edu.cn (H.Y.); Tel.: +86-731-88830549 (H.Y.)

Received: 24 January 2018; Accepted: 7 March 2018; Published: 9 March 2018

Abstract: Kaolinite (Kaol) was intercalated with dimethyl sulfoxide (DMSO) and subsequently methanol (MeOH) to prepare intercalation compounds Kaol-DMSO and Kaol-MeOH. Kaol-MeOH was used as an intermediate to synthesize Kaol-sodium dodecyl sulfate (SDS) intercalation compound (Kaol-SDS) via displacement reaction. The ultrasonic exfoliation of Kaol-SDS produced a resultant Kaol-SDS-U. The samples were characterized by X-ray diffraction (XRD), Fourier transformation infrared spectroscopy (FTIR), thermal analysis, scanning electronic microscopy (SEM), transmission electron microscopy (TEM) and particle size analysis. The results revealed that the intercalation of sodium dodecyl sulfate into kaolinite layers caused an obvious increase of the basal spacing from 0.72–4.21 nm. The dehydroxylation temperature of Kaol-SDS was obviously lower than that of original kaolinite. During the intercalation process of sodium dodecyl sulfate, a few kaolinite layers were exfoliated and curled up from the edges of the kaolinite sheets. After sonication treatment, the kaolinite layers were further transformed into nanoscrolls, and the exfoliated resultant Kaol-SDS-U possessed a smaller particle size close to nanoscale.

Keywords: kaolinite; intercalation; exfoliation; sodium dodecyl sulfate

1. Introduction

Recently, rubber/layered silicate nanocomposites have attracted extensive interest both in industry and academia due to the unique characteristics of nano-sized layered silicates, including their large surface area, high surface reactivity and relatively low cost [1–4]. The layered silicates used in rubbers can increase mechanical properties, improve thermal resistance and reduce gas permeability [2,5,6]. It is well known that layered silicates with large aspect ratios added in rubber are more beneficial to increase the tortuosity of the diffusive path for the gas molecule, providing excellent barrier properties [2,7,8]. However, the raw layered silicates have a disc-like structure with a low aspect ratio. Therefore, many efforts have been made to increase the aspect ratio of layer silicates [9–13].

Kaolinite (Kaol), $\text{Al}_2\text{Si}_2\text{O}_5(\text{OH})_4$, is a typical 1:1 layered dioctahedral aluminum silicate, which has been widely used as a filler in rubber [6,14–17]. The layers of kaolinite are composed of SiO_4 tetrahedral sheets linked to $\text{AlO}_2(\text{OH})_4$ octahedral sheets. The adjacent layers are tightly held together by hydrogen bonds between hydroxyl groups on the octahedral (aluminum) sheets and the tetrahedral (silicon) sheets. In order to increase the accessible aspect ratio of kaolinite, many methods have been used to exfoliate the stack layers of kaolinite, such as intercalation, mechanical exfoliation and assisted sonication [18–21]. Among these exfoliation methods, intercalation has received considerable attention because the intercalated molecules could not only weaken the hydrogen bonding, but also provide space for kaolinite to be exfoliated [19,22,23]. Nevertheless, only a limited number of polar guest

species can be intercalated directly into kaolinite, such as urea [24,25], potassium acetate [26–29] and dimethyl sulfoxide [30,31]. Moreover, kaolinite would not be exfoliated even though these species were intercalated into kaolinite layers due to the strong inner hydrogen bonds between the layers.

Actually, natural minerals have been widely used for the preparation of advanced materials [32–46]. Much work has been done to demonstrate that various intercalated guest species can be extended by the “displacement method”. Especially the methoxy-modified kaolinite shows more versatility for further intercalation reactions. For example, Komori et al. reported that kaolinite-alkylamines intercalation compounds were prepared by using the methanol-treated kaolinite intercalation as an intermediate [47,48]. The results showed that the basal spacing increased up to 5.75 nm when octadecylamine was used. Matusik et al. prepared kaolinite intercalation compounds with benzylalkylammonium chlorides [49,50]. They have reported that a methoxy-modified kaolinite was used as a precursor, which had OCH_3 methoxyl groups attached to the octahedral sheet. Additionally, Gardolinski and Lagaly [51,52] reported that *n*-hexylamine, *n*-octadecylamine and *n*-docosanamine were intercalated into the layers of kaolinite by the same method reported by Komori and co-workers [47,48]. When *n*-docosanamine was used, the largest basal spacing of 6.42 nm was obtained, and the platy layers transformed into nanoscrolls after the deintercalation performed with toluene. Kuroda et al. also reported that some quaternary ammonium salts intercalated into the interlayers of kaolinite using methoxy-modified kaolinite as an intermediate, and most of the exfoliated kaolinite layers also transformed into nanoscrolls [19]. Liu et al. demonstrated kaolinite layers got curled up into one-dimensional nanoscrolls automatically when they are exfoliated in methanol after intercalation with alkyltrimethylammonium salts [53]. This depicted the morphological change of kaolinite layers during intercalation and exfoliation.

The guest species mentioned above were defined as cationic intercalators, because they could be ionized to produce cations. In the case of intercalation, after kaolinite stacking layers reacted with cationic long chain intercalators, the layer-to-layer distance expanded, and the binding forces of adjacent layers decreased significantly. The kaolinite layers were lastly exfoliated and curled up into nanoscrolls. Therefore, it is not a good way to obtain kaolinite with a high aspect ratio. Based on the literature described above, little attention has been paid to the intercalation of kaolinite with anionic guest species. Sidheswaran et al. [54] firstly examined the preparation of intercalation compounds of kaolinite by a one-step displacement method with the salts of long-chain fatty acids. The results indicated that the expanded basal spacing of kaolinite was independent of the chain length of guest species, because the basal spacing of kaolinite expanded from 0.7–1.1 nm. Wang et al. [55] recently reported that the interlayer spacing of kaolinite was enlarged to 4.55–4.79 nm intercalated by sodium stearate using the methoxy-modified kaolinite as the precursor.

In this work, as an important anionic surfactant, SDS was intercalated into kaolinite layers using Kaol-MeOH as the initial material first. Afterwards, the Kaol-SDS was treated by the sonication method. It was found that the morphology of most exfoliated kaolinite layers remained intact. The exfoliation method may provide the possibility of preparing thin kaolinite flakes with large aspect ratios.

2. Materials and Methods

2.1. Materials

The kaolinite (Kaol) used in the present study with a Hinckley index of 1.31, obtained from Zhangjiakou, China, was used as received. The chemical composition of purified kaolinite is listed in Table 1. Dimethyl sulfoxide (DMSO) and methanol (MeOH) were obtained from Xilong Chemical Co., Ltd., Beijing, China. Sodium dodecyl sulfate (SDS) was provided by Sinopharm Chemical Regent Co., Ltd., Beijing, China. Hydrochloric acid (HCl) was purchased from Beijing Chemical Plant (Beijing, China). All reagents were of analytical-grade purity (>99.0%) and used as received.

Table 1. Chemical composition of kaolinite (Kaol) obtained from Zhangjiakou.

Composition	SiO ₂	Al ₂ O ₃	Fe ₂ O ₃	TiO ₂	MgO	CaO	Na ₂ O	K ₂ O	P ₂ O ₅	LOI
Content (mass %)	44.64	38.05	0.22	1.13	0.06	0.11	0.27	<0.10	0.13	15.06

LOI: loss on ignition.

2.2. Preparation

To prepare the methoxy-modified Kaol (Kaol-MeOH), the DMSO intercalated Kaol (denoted as Kaol-DMSO) was prepared according to the previous reports [30,31]. Afterwards, preintercalates were mixed with methanol and stirred for 10 days at room temperature. The solution was replaced by fresh methanol every day. Then, the precipitates were centrifuged and closed in a sealed vessel to prevent methanol evaporation. To prepare the SDS intercalated Kaol, 1 g of wet Kaol-MeOH was dispersed in 20 mL of 1.0 mol/L sodium dodecyl sulfate (SDS) aqueous solutions. The pH value of the mixture was adjusted to 2 with 1.0 M HCl solution and stirred at 60 °C for 72 h. Then, the solid in the mixture was collected by centrifugation and washed thoroughly with distilled water. The successfully prepared kaolinite-sodium dodecyl sulfate intercalation compound was denoted Kaol-SDS. At last, 1 g Kaol-SDS was mixed with 200 mL of 0.1 mol/L SDS solutions and stirred vigorously for 0.5 h. Then, the resulting mixture was tip sonicated for 2 h using a Biaosafer ultrasonic cell disrupter at 800 W under ambient conditions. At last, the ultrasonic product was collected for characterization and designated as Kaol-SDS-U.

2.3. Characterization

Powder XRD patterns were obtained by a Rigaku D/max 2500PC X-ray diffractometer (RIGAKU Company, Akishima, Japan) with CuK α (λ = 0.154178 nm) radiation at the scanning rate of 1°/min in the 2 θ range of 1–15°, operating at 40 kV and 100 mA. Typically, the samples were firstly dispersed in absolute ethyl alcohol. Then, about 1 mL of the mixture was dropped on a glass and allowed to air dry. The prepared glass was used for the test. The infrared spectra were collected using a Nicolet Nexus 870 FTIR spectrometer (Thermo Company, Waltham, MA, USA) with a smart endurance single-bounce diamond ATR cell. We transformed the corresponding data into transmission data by using the ONMIC software between 600 and 4000 cm^{−1}, with a resolution of 4 cm^{−1} and 32 scans. Thermal analysis was recorded with a Mettler Toledo TGA/DSC1/1600HT instrument (Mettler-Toledo Company, Zurich, Switzerland), operated at a heating rate of 10 °C/min from room temperature to 1100 °C under a nitrogen gas atmosphere. Samples for TEM were prepared from dilute suspensions and investigated using a FEI-Tecnaï G2 F30 S-TWIN TEM (FEI Company, Eindhoven, The Netherlands) operating at 300 kV. The powder samples were dispersed in ethanol by ultrasound for 20 min and then deposited on holey carbon-coated copper grids. Samples for SEM were prepared by gold-coating powders and analyzed with a Hitachi S-4800 SEM (accelerating voltage of 3 kV, Hitachi High-Technologies Company, Tokyo, Japan). The particle size distribution of the samples was measured with the Malvern Mastersizer 2000. The measurements (Malvern Instruments Ltd, Malvern, UK) were conducted in liquid dispersion, i.e., in distilled water with a refractive index for light equal to 1.55. Cycle injection mode was selected, and test times were 1~2 min.

3. Results and Discussion

3.1. XRD Analysis

Figure 1 shows the XRD patterns of Kaol, Kaol-DMSO, Kaol-MeOH and Kaol-SDS. In the case of Kaol, the (001) reflection can be observed at 12.24 (2 θ) with basal spacing of 0.72 nm. After being intercalated with DMSO, a new reflection appeared at 1.14 nm, corresponding to a typical interlayer distance of Kaol-DMSO as described before [30,31]. When the Kaol-DMSO was washed with fresh MeOH, MeOH gradually grafted on to the inner-surface hydroxyls of Kaol by an Al–O–C bond [56].

The basal spacing of 0.86 nm of Kaol-MeOH was observed after drying (Figure 1). Upon intercalation of SDS, the basal spacing of Kaol-MeOH increased to 4.21 nm, which was an increase of 3.49 nm compared to Kaol, indicating the successful intercalation of SDS into Kaol. Additionally, the reflections at 2.07 nm and 1.36 nm are assigned to the second and third order diffractions of Kaol-SDS, respectively.

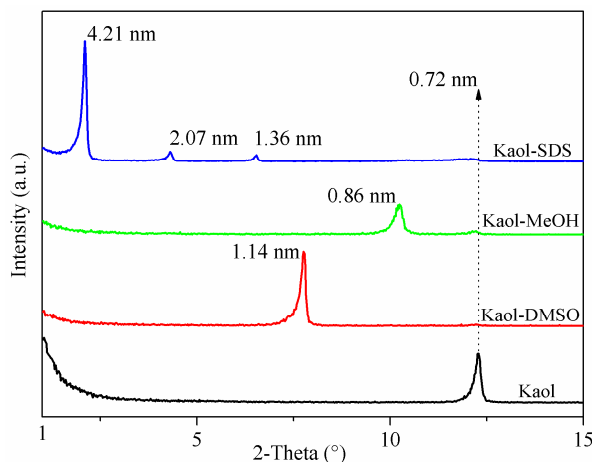


Figure 1. XRD patterns of Kaol and the intercalated Kaol products.

3.2. FTIR Analysis

FTIR spectra of Kaol, Kaol-DMSO, Kaol-MeOH and Kaol-SDS with no further treatment are shown in Figure 2. The FTIR spectrum of Kaol was characterized by hydroxyl stretching peaks at 3690 cm^{-1} and 3620 cm^{-1} . A shoulder of the large 3690 cm^{-1} at around 3665 cm^{-1} could be clearly observed in the raw Kaol. The band at 3620 cm^{-1} was assigned to the inner hydroxyl of Kaol. The other bands corresponded to inner-surface hydroxyl. Generally, the inner hydroxyl groups are not influenced by the intercalation and grafting due to the hydrogen of inner hydroxyls being oriented towards the vacant sites. However, the inner-surface hydroxyls are readily affected by the interlayer modifications. When DMSO was intercalated, the band at 3690 cm^{-1} shifted to 3695 cm^{-1} , while the band at 3665 shifted to 3660 cm^{-1} (Figure 2). The new bands at 3536 and 3505 cm^{-1} were due to the formation of moderately strong hydrogen bonding between some of the inner surface hydroxyls and the sulphonyl oxygen [57]. Besides, the characteristic stretching vibrations of C–H at 3023 cm^{-1} (asymmetry) and 2937 cm^{-1} (symmetry) corresponded to $-\text{CH}_2$ of DMSO. The Si–O bond stretching bands of Kaol at 1115 , 1029 and 1007 cm^{-1} were observed at 1123 , 1025 and 1109 cm^{-1} for Kaol-DMSO. Additionally, the Al–OH bending vibrations of Kaol at 912 cm^{-1} shifted to 904 cm^{-1} .

Then, after the Kaol-DMSO was washed 10 times with fresh MeOH, the C–H stretching bands of DMSO vanished completely, due to the removal of excess DMSO. By the intercalation of DMSO, the bands at 3695 cm^{-1} appeared. After treatment with fresh MeOH, this band was weakened. Compared with Kaol-DMSO, The Si–O stretching band of Kaol-MeOH at 1040 cm^{-1} appeared again. All the changes of bands were attributed to the deintercalation of Kaol-DMSO and intercalation of Kaol with MeOH. As seen in the FTIR spectrum of Kaol-SDS, the bands of inner-surface hydroxyl groups have no obvious changes. The band at 3693 cm^{-1} was attributed to the tiny shift of the hydroxyl stretching band to 3692 cm^{-1} (Figure 2). Additionally, a new inconspicuous band at 3542 cm^{-1} may be due to SDS hydrogen bonded to hydroxyl surface groups. In comparison with Kaol-MeOH, the characteristic bands of Kaol-SDS were shown at 2915 , 2850 , 1652 , 1556 and 1472 cm^{-1} . The first two bands originated from the $-\text{CH}_2$ of SDS corresponding to the asymmetry and symmetry stretching bands, respectively. The absorption band at 1472 cm^{-1} was ascribed to the C–O stretching band. On the other hand, the variation of the Si–O stretching band was not obvious. Therefore, the FTIR spectra variations

of Kaol-SDS further confirmed the successful intercalation of SDS into kaolinite, which was in good agreement with the XRD analyses.

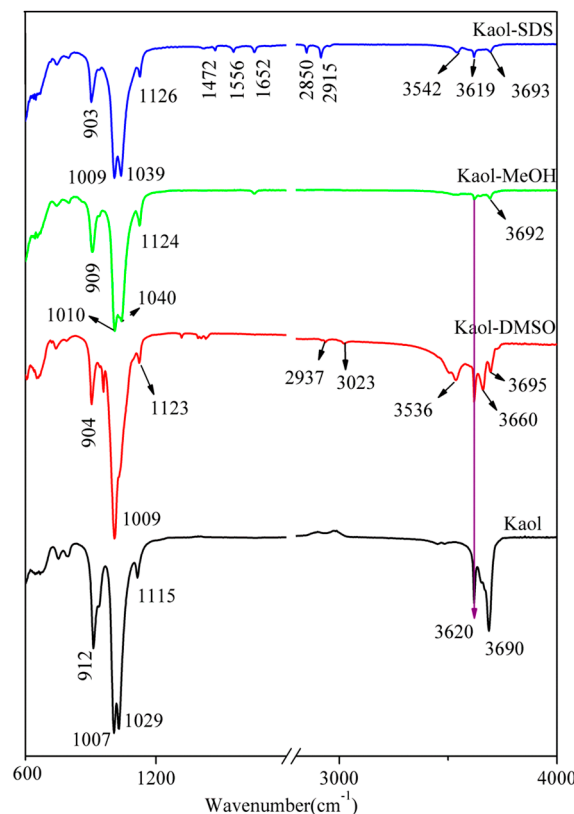


Figure 2. FTIR spectra of Kaol, Kaol-DMSO, Kaol-MeOH and Kaol-SDS.

3.3. Thermal Analysis

The TG/DTG curves of Kaol and its intercalation compounds are shown in Figure 3. In order to investigate the dehydroxylation of Kaol with different treatments, the DTG effect was characterized by extrapolating the temperature of the beginning of the peak (T_i), ending of the peak (T_e) and width of the peak ($W = T_e - T_i$). The temperatures of T_i (onset) and T_e (outset) were determined from the intersection of the extrapolated initial baseline and tangent to the frontal and terminal inflection points, respectively. The DTG peaks parameters of the dehydroxylation of Kaol and Kaol intercalation compounds are presented in Table 2. The thermal decomposition of Kaol occurred only in one step observed in the TG curve. This step started at 450 °C and terminated at 600 °C and was related to the dehydroxylation of Kaol. The DTG peak of Kaol centered at 520 °C was clearly observed, where a mass loss of 12.6% was attained.

As seen in the TG curve of Kaol-DMSO, there were two steps, for which the first (5.9% mass loss) took place between 120 and 220 °C was contributed to the volatilization of DMSO. The second step (3.8% mass loss) that occurred between 455 °C and 630 °C was assigned to the dehydroxylation of Kaol. The DTG maximum of the two processes appeared at 200 and 524 °C, respectively. In comparison with Kaol, while the intercalated Kaol with DMSO did not modify the temperature of the DTG maximum of the dehydroxylation, and the width of the peak decreased (Figure 3, Table 2). From the TG curve of Kaol-MeOH, a strong endothermic peak starting at 400 °C and ending at 600 °C was observed, with a mass loss of 2.2%. A less obvious endothermic peak appearing between 60 and 200 °C was also displayed, which contributed to a mass loss of 12.5%, attributed to the degradation of water, MeOH and methoxy groups in Kaol layers. The reason that the first peak in the DTG curve of Kaol-MeOH became seriously broadened was the stronger interaction between MeOH and the hydroxyl of Kaol.

In comparison with Kaol and Kaol-DMSO, the DTG peak of Kaol-MeOH shifted to a lower temperature (Table 2), which was due to the hydroxyl activation.

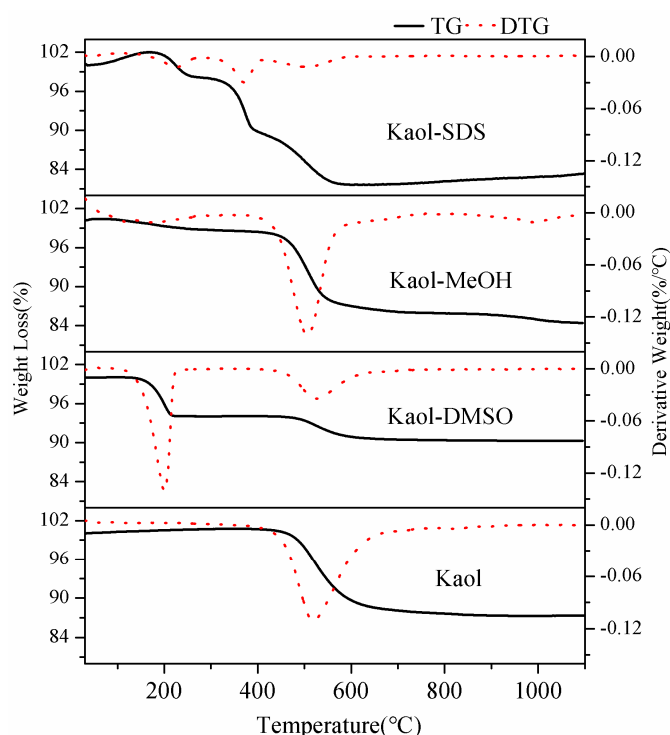


Figure 3. TG /DTG curves of Kaol, Kaol-DMSO, Kaol-MeOH and Kaol-SDS.

Table 2. The corresponding parameters of the dehydroxylation of Kaol and its intercalation compounds.

Samples	DTG Peak (°C)	Ti (°C)	Te (°C)	W (°C)
Kaol	520	450	632	182
Kaol-DMSO	524	456	627	171
Kaol-MeOH	507	440	564	124
Kaol-SDS	502	406	587	181

Four mass losses were observed in the DTG curve of Kaol-SDS, while three main processes were detected in the TG curve. Typically, the first decomposition process occurred below 80 °C, which was ascribed to the removal of externally-absorbed water. Then, the second loss, corresponding to the degradation of external SDS, was observed in the range of 135–275 °C. The third volatilization, which represented the removal of sodium dodecyl sulfate located in the Kaol interlamellar space, occurred between 305 and 410 °C. Lastly, the loss starting at 420 and ending at 600 °C was attributed to the dehydroxylation of Kaol. It was noteworthy that the dehydroxylation of Kaol-SDS appeared at 502 °C, which was the lowest of all samples, indicating that the activity of hydroxyl groups of Kaol was increased by the intercalation with SDS. This was probably due to the effect of intercalated SDS.

3.4. Particle Size and Morphology Analysis

Figure 4 demonstrates the morphologies of Kaol and Kaol products with different treatments. The raw Kaol was mainly composed of typical stacks of hexagonal, large sheet-like and fine-grained particles (Figure 4a). Compared with the original Kaol, no significant changes were observed in the morphology of Kaol-MeOH due to the small interlayer space of Kaol. After the intercalation of SDS, however, the *d* spacing of Kaol reached up to 4.21 nm, and the Kaol layers were simultaneously

exfoliated (Figure 4e); because it was obviously found that low aggregated silicate layers were shown and some platy particles scrolled from the edges of Kaol (Figure 4e).

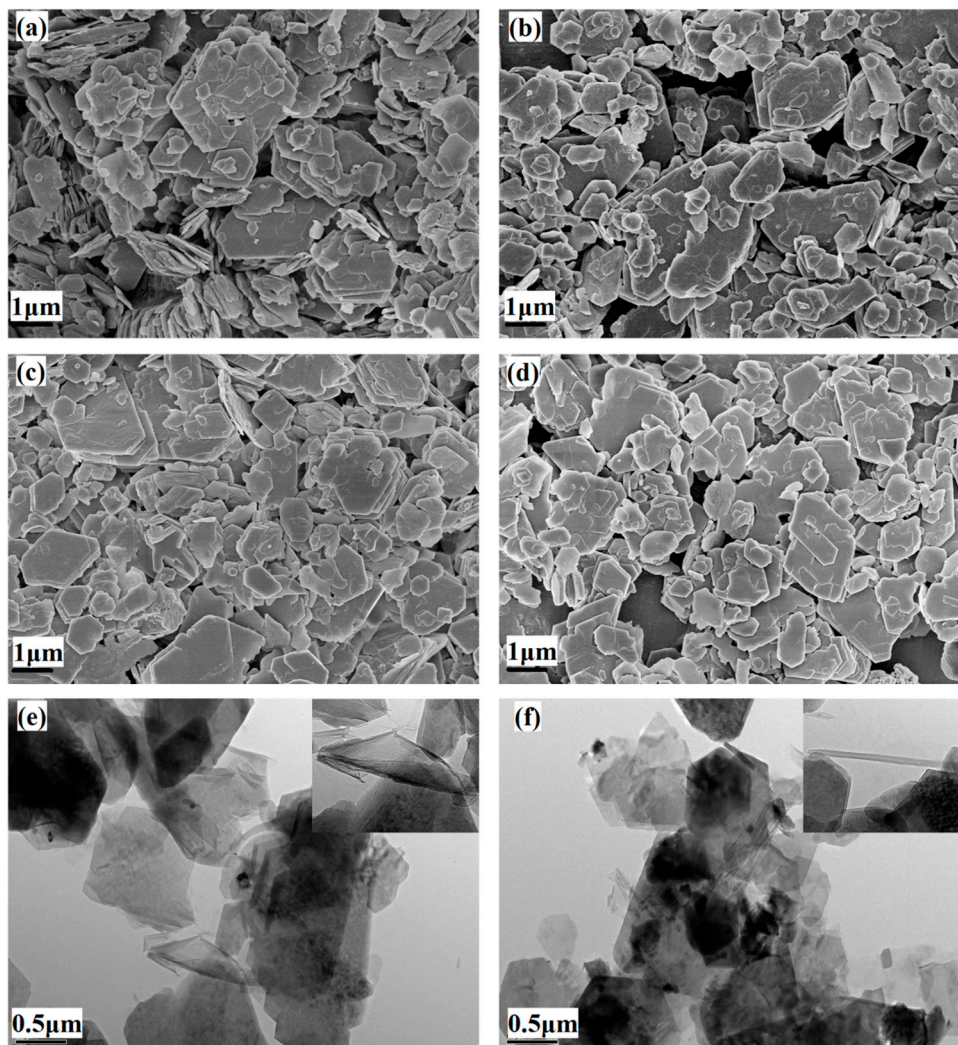


Figure 4. SEM images of (a) Kaol, (b) Kaol-MeOH, (c) Kaol-SDS and (d) Kaol-SDS-U; TEM images of (e) Kaol-SDS and (f) Kaol-SDS-U.

Figure 4d displays the morphology of exfoliated Kaol-SDS, which was treated by sonication. In comparison with Kaol-SDS, the SEM images of Kaol-SDS-U also showed nearly no changes. However, the curl degree of the Kaol layer was more serious than that of the Kaol layer without ultrasonication (Figure 4f). Furthermore, completely curled layers are shown in the highly magnified TEM image, indicating that a few Kaol layers would transform into nanoscrolls during the exfoliation process. Previous studies [19,52,58–60] suggested that abundant kaolinite layers would be transformed into nanoscrolls after the intercalation with long chain cationic intercalators such as cetyltrimethylammonium bromide (CTAB), octadecyl dimethyl ammonium chloride (OTAC) and dodecylamine. In comparison with Kaol-SDS and Kaol-SDS-U, however, only a limited number of Kaol layers transformed into nanoscrolls. Most Kaol layers were composed of euhedral particles with a pseudohexagonal morphology.

In order to analyze the particle size variations directly, all samples were characterized by a Malvin particle size test instrument. The grain-size frequency curves of Kaol, Kao-MeOH, Kaol-SDS and Kaol-SDS-U are shown in Figure 5 and Table 3. When raw Kaol was intercalated by DMSO and MeOH

in turn, the distribution peaks shifted to a small size (Figure 5a,b), and the mean particle diameter of Kaol-MeOH decreased nearly two times (Table 3). In the case of Kaol-SDS, both the size distribution and parameters were similar to Kaol-MeOH, indicating that most Kaol layers were not exfoliated due to the intercalation with SDS. After sonication, however, the particle size of Kaol-SDS was further reduced (Table 3). At the same time, there are two obvious distribution peaks (Figure 5d), suggesting two main particle size ranges in the samples.

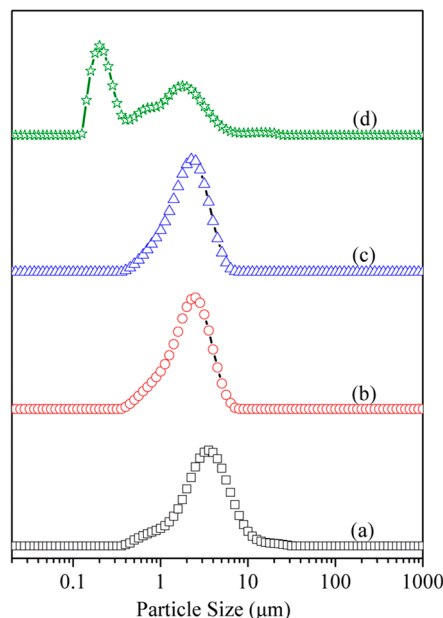


Figure 5. Particle size distribution curves of (a) Kaol, (b) Kaol-MeOH, (c) Kaol-SDS and (d) Kaol-SDS-U.

Table 3. The particle size of raw Kaol and Kaol with different exfoliation methods.

Samples	D ₁₀ (μm) ^a	D ₅₀ (μm) ^a	D ₉₀ (μm) ^a	D _{average} (μm)
Kaol	1.225	3.142	6.614	3.729
Kaol-MeOH	0.885	2.054	3.702	2.205
Kaol-SDS	0.885	1.955	3.507	2.104
Kaol-SDS-U	0.165	0.635	2.811	1.274

^a D₁₀, D₅₀ and D₉₀ indicate the diameters at 10%, 50% and 90% of the cumulative volume distribution, respectively.

The results of the morphology and particle size of Kaol with different treatments indicated that although the intercalation of Kaol with SDS expanded the interlayer space, very few Kaol layers were exfoliated. The Kaol-SDS under sonication seriously reduced the average grain size of Kaol, while the platelets were broken into small ones. Moreover, it was easily noted that the particle size of the exfoliated Kaol layers via sonication was closer to the nanoscale.

4. Conclusions

Kaol-SDS has been successfully prepared by using Kaol-MeOH as an intermediate. The XRD analyses indicated that the basal spacing of Kaol expanded to 4.21 nm after intercalation with SDS. From the thermal analyses, it was found that the dehydroxylation temperature of Kaol-SDS evenly reduced, maybe due to the hydroxyl activation of Kaol. The morphology analysis confirmed that few layers of Kaol-MeOH were exfoliated, and few partially-curved Kaol sheets occurred in the intercalation procedures. The sonication of Kaol-SDS further exfoliated Kaol layers into very thin sheets that curled up to form nanoscrolls. However, most of the Kaol layers remained intact. Based on the particle size analysis, the average grain size of Kaol-SDS-U decreased greatly in comparison with Kaol-SDS, and

some Kaol layers were close to the nanoscale. Thus, it could be hopeful to provide a new exfoliation method to obtain large aspect ratios of Kaol layers.

Acknowledgments: This work was supported by the National Nature Science Foundation of China (51034006), the National Key R&D Program of China (2017YFB0310903), the Key R&D Program of Hunan Province (2017GK2251) and the Central South University Graduate Independent Exploration Innovation Program (2017zzts191).

Author Contributions: Qinfu Liu and Shilong Zhang conceived of the project. Xiaochao Zuo wrote the initial drafts of the work. Qinfu Liu and Huaming Yang wrote the final paper. Xiaochao Zuo designed and performed the experiments and characterized the samples. Xiaochao Zuo and Ding Wang analyzed the data. All authors discussed the results and commented on the manuscript.

Conflicts of Interest: The authors declare no conflict of interest.

References

1. Kotal, M.; Bhowmick, A.K. Polymer nanocomposites from modified clays: Recent advances and challenges. *Prog. Polym. Sci.* **2015**, *51*, 127–187. [\[CrossRef\]](#)
2. Cui, Y.B.; Kumar, S.; Kona, B.R.; van Houcke, D. Gas barrier properties of polymer/clay nanocomposites. *RSC Adv.* **2015**, *5*, 63669–63690. [\[CrossRef\]](#)
3. Zhang, Y.D.; Liu, Q.F.; Xiang, J.J.; Zhang, S.L.; Frost, R.L. Influence of the structural characteristic of pyrolysis products on thermal stability of styrene-butadiene rubber composites reinforced by different particle sized kaolinites. *J. Therm. Anal. Calorim.* **2014**, *117*, 1201–1210. [\[CrossRef\]](#)
4. Bromberg, L.; Straut, C.M.; Centrone, A.; Wilusz, E.; Hatton, T.A. Montmorillonite functionalized with pralidoxime as a material for chemical protection against organophosphorous compounds. *ACS Appl. Mater. Interface* **2011**, *3*, 1479–1484. [\[CrossRef\]](#) [\[PubMed\]](#)
5. Zhang, Y.D.; Liu, Q.F.; Zhang, Q.; Lu, Y.P. Gas barrier properties of natural rubber/kaolin composites prepared by melt blending. *Appl. Clay Sci.* **2010**, *50*, 255–259. [\[CrossRef\]](#)
6. Yahaya, L.E.; Adebawale, K.O.; Menon, A.R.R. Mechanical properties of organomodified kaolin/natural rubber vulcanizates. *Appl. Clay Sci.* **2009**, *46*, 283–288. [\[CrossRef\]](#)
7. Mirzadeh, A.; Kokabi, M. The effect of composition and draw-down ratio on morphology and oxygen permeability of polypropylene nanocomposite blown films. *Eur. Polym. J.* **2007**, *43*, 3757–3765. [\[CrossRef\]](#)
8. Cabeda, L.; Gimenez, E.; Lagaron, J.M.; Gavara, R.; Saura, J.J. Development of EVOH-kaolinite nanocomposites. *Polymer* **2004**, *45*, 5233–5238. [\[CrossRef\]](#)
9. Bundy, W.; Ishley, J. Kaolin in paper filling and coating. *Appl. Clay Sci.* **1991**, *5*, 397–420. [\[CrossRef\]](#)
10. Xia, X.N.; Zeng, X.L.; Liu, J.; Xu, W.J. Preparation and characterization of epoxy/kaolinite nanocomposites. *J. Appl. Polym. Sci.* **2010**, *118*, 2461–2466. [\[CrossRef\]](#)
11. Cheng, H.F.; Zhang, Z.L.; Liu, Q.F.; Leung, J. A new method for determining platy particle aspect ratio: A kaolinite case study. *Appl. Clay Sci.* **2014**, *97–98*, 125–131. [\[CrossRef\]](#)
12. Lu, C.S.; Mai, Y.W. Influence of aspect ratio on barrier properties of polymer-clay nanocomposites. *Phys. Rev. Lett.* **2005**, *95*, 1–4. [\[CrossRef\]](#) [\[PubMed\]](#)
13. Zhang, S.L.; Liu, Q.F.; Yang, Y.J.; Wang, D.; He, J.K.; Sun, L.Y. Preparation; morphology; and structure of kaolinites with various aspect ratios. *Appl. Clay Sci.* **2017**, *147*, 117–122. [\[CrossRef\]](#)
14. Zoromba, M.S.; Belal, A.A.M.; Ali, A.E.M.; Helaly, F.M.; Abd El-Hakim, A.A.; Badran, A.S. Preparation and characterization of some NR and SBR formulations containing different modified kaolinite. *Polym. Plast. Technol. Eng.* **2007**, *46*, 529–535. [\[CrossRef\]](#)
15. Zhang, Y.D.; Zhang, Q.; Liu, Q.F.; Cheng, H.F.; Frost, R.L. Thermal stability of styrene butadiene rubber (SBR) composites filled with kaolinite/silica hybrid filler. *J. Therm. Anal. Calorim.* **2014**, *115*, 1013–1020. [\[CrossRef\]](#)
16. Zhang, Y.M.; Liu, Q.F.; Zhang, S.L.; Zhang, Y.D.; Zhang, Y.F.; Liang, P. Characterization of kaolinite/styrene butadiene rubber composite: Mechanical properties and thermal stability. *Appl. Clay Sci.* **2016**, *124–125*, 167–174. [\[CrossRef\]](#)
17. Zhang, Q.; Liu, Q.F.; Zhang, Y.D.; Cheng, H.F.; Lu, Y.P. Silane-grafted silica-covered kaolinite as filler of styrene butadiene rubber. *Appl. Clay Sci.* **2012**, *65–66*, 134–138. [\[CrossRef\]](#)
18. Cheng, H.F.; Liu, Q.F.; Zhang, J.S.; Yang, J.; Frost, R.L. Delamination of kaolinite-potassium acetate intercalates by ball-milling. *J. Colloid Interface Sci.* **2010**, *348*, 355–359. [\[CrossRef\]](#) [\[PubMed\]](#)

19. Kuroda, Y.; Ito, K.; Itabashi, K.; Kuroda, K. One-Step Exfoliation of kaolinites and their transformation into nanoscrolls. *Langmuir* **2011**, *27*, 2028–2035. [[CrossRef](#)] [[PubMed](#)]
20. Nicolosi, V.; Chhowalla, M.; Kanatzidis, M.G.; Strano, M.S.; Coleman, J.N. Liquid exfoliation of layered materials. *Science* **2013**, *340*, 1226419. [[CrossRef](#)]
21. Pi, Z.B.; Liu, Z.Q.; Yang, C.; Tian, X.K.; Fei, J.B.; Zheng, J.H. Exfoliation of kaolinite by urea-intercalation precursor and microwave irradiation assistance process. *Front. Earth Sci. China* **2007**, *1*, 26–29. [[CrossRef](#)]
22. Li, X.G.; Liu, Q.F.; Cheng, H.F.; Zhang, S.; Frost, R.L. Mechanism of kaolinite sheets curling via the intercalation and delamination process. *J. Colloid Interface Sci.* **2015**, *444*, 74–80. [[CrossRef](#)] [[PubMed](#)]
23. Zuo, X.C.; Wang, D.; Zhang, S.L.; Liu, Q.F.; Yang, H.M. Effect of intercalation agents on morphology of exfoliated kaolinite. *Minerals* **2017**, *7*, 249. [[CrossRef](#)]
24. Makó, É.; Kristóf, J.; Horváth, E.; Vágvölgyi, V. Kaolinite-urea complexes obtained by mechanochemical and aqueous suspension techniques—A comparative study. *J. Colloid Interface Sci.* **2009**, *330*, 367–373. [[CrossRef](#)] [[PubMed](#)]
25. Cheng, H.F.; Liu, Q.F.; Liu, J.; Sun, B.; Kang, Y.X.; Frost, R.L. TG-MS-FTIR (evolved gas analysis) of kaolinite-urea intercalation complex. *J. Therm. Anal. Calorim.* **2014**, *116*, 195–203. [[CrossRef](#)]
26. Long, M.; Zhang, Y.; Shu, Z.; Tang, A.D.; Ouyang, J.; Yang, H.M. Fe₂O₃ nanoparticles anchored on 2D kaolinite with enhanced antibacterial activity. *Chem. Commun.* **2017**, 5346, 6255–6258. [[CrossRef](#)] [[PubMed](#)]
27. Long, M.; Zhang, Y.; Huang, P.; Chang, S.; Hu, Y.H.; Yang, Q.; Mao, L.F.; Yang, H.M. Emerging nanoclay composite for effective hemostasis. *Adv. Funct. Mater.* **2017**. [[CrossRef](#)]
28. Zhang, Y.; Long, M.; Huang, P.; Chang, S.; Hu, Y.H.; Yang, H.M.; Tang, A.D.; Mao, L.F. Intercalated 2D nanoclay for emerging drug delivery in cancer therapy. *Nano Res.* **2017**, *10*, 2633–2643. [[CrossRef](#)]
29. Frost, R.L.; Kristof, J.; Paroz, G.N.; Klopogge, J.T. Modification of the kaolinite hydroxyl surfaces through intercalation with potassium acetate under pressure. *J. Colloid Interface Sci.* **1998**, *208*, 478–486. [[CrossRef](#)] [[PubMed](#)]
30. Liu, S.Y.; Yang, H.M. Composite of coal-series kaolinite and capric-lauric acid as form-stable phase-change material. *Energy Technol.* **2015**, *3*, 77–83. [[CrossRef](#)]
31. Zhang, S.; Liu, Q.F.; Cheng, H.F.; Zeng, F.G. Combined experimental and theoretical investigation of interactions between kaolinite inner surface and intercalated dimethyl sulfoxide. *Appl. Surf. Sci.* **2015**, *331*, 234–240. [[CrossRef](#)]
32. Fu, L.J.; Yang, H.M. Structure and electronic properties of transition metal doped kaolinite nanoclay. *Nanoscale Res. Lett.* **2017**, *12*, 1–7. [[CrossRef](#)] [[PubMed](#)]
33. Yan, Z.L.; Fu, L.J.; Hu, Y.H.; Yang, H.M. Functionalized 2D Clay derivative: Hybrid nanosheets with unique lead sorption behaviors and interface structure. *Adv. Mater. Interface* **2017**. [[CrossRef](#)]
34. Yan, Z.L.; Fu, L.J.; Zuo, X.C.; Yang, H.M. Green assembly of stable and uniform silver nanoparticles on 2D silica nanosheets for catalytic reduction of 4-nitrophenol. *Appl. Catal. B Environ.* **2018**, *226*, 23–30. [[CrossRef](#)]
35. Yan, Z.L.; Fu, L.J.; Zuo, X.C.; Yang, H.M.; Ouyang, J. Amino-functionalized Hierarchical Porous SiO₂-AlOOH Composite Nanosheets with Enhanced Adsorption Performance. *J. Hazard. Mater.* **2018**, *344*, 1090–1100. [[CrossRef](#)]
36. Fu, L.J.; Yang, H.M.; Hu, Y.H.; Wu, D.; Navrotsky, A. Tailoring mesoporous γ -Al₂O₃ properties by transition metal doping: A combined experimental and computational study. *Chem. Mater.* **2017**, *29*, 1338–1349. [[CrossRef](#)]
37. Yan, Z.L.; Yang, H.M.; Ouyang, J.; Tang, A.D. In situ loading of highly-dispersed CuO nanoparticles on hydroxyl-group-rich SiO₂-AlOOH composite nanosheets for CO catalytic oxidation. *Chem. Eng. J.* **2017**, *316*, 1035–1046. [[CrossRef](#)]
38. Peng, K.; Fu, L.J.; Li, X.Y.; Ouyang, J.; Yang, H.M. Stearic acid modified montmorillonite as emerging microcapsules for thermal energy storage. *Appl. Clay Sci.* **2017**, *138*, 100–106. [[CrossRef](#)]
39. Liu, S.Y.; Yan, Z.L.; Fu, L.J.; Yang, H.M. Hierarchical nano-activated silica nanosheets for thermal energy storage. *Sol. Energy Mater. Sol. Cells* **2017**, *167*, 140–149. [[CrossRef](#)]
40. Shu, Z.; Zhang, Y.; Yang, Q.; Yang, H.M. Halloysite nanotubes supported Ag and ZnO nanoparticles with synergistically enhanced antibacterial activity. *Nanoscale Res. Lett.* **2017**, *12*, 1–7. [[CrossRef](#)] [[PubMed](#)]
41. Hou, K.; Wen, X.; Yan, P.; Tang, A.D.; Yang, H.M. Tin oxide-carbon coated sepiolite nanofibers with enhanced lithium-ion storage property. *Nanoscale Res. Lett.* **2017**, *12*, 1–10. [[CrossRef](#)] [[PubMed](#)]

42. Jin, J.; Ouyang, J.; Yang, H.M. Pd nanoparticles and MOFs synergistically hybridized halloysite nanotubes for hydrogen storage. *Nanoscale Res. Lett.* **2017**, *12*, 1–9. [[CrossRef](#)] [[PubMed](#)]
43. Hou, K.; Ouyang, J.; Zheng, C.H.; Zhang, J.H.; Yang, H.M. Chemically modified sepiolite fibers for reinforcing resin brake composites. *Mater. Express* **2017**, *7*, 104–112. [[CrossRef](#)]
44. Shen, Q.; Ouyang, J.; Zhang, Y.; Yang, H.M. Lauric acid/modified sepiolite composite as a form-stable phase change material for thermal energy storage. *Appl. Clay Sci.* **2017**, *146*, 14–22. [[CrossRef](#)]
45. Peng, K.; Yang, H.M. Carbon hybridized montmorillonite nanosheets: Preparation, structural evolution and enhanced adsorption performance. *Chem. Commun.* **2017**, *53*, 6085–6088. [[CrossRef](#)] [[PubMed](#)]
46. Fu, L.J.; Yang, H.M.; Tang, A.D.; Hu, Y.H. Engineering a tubular mesoporous silica nanocontainer with well-preserved clay shell from natural halloysite. *Nano Res.* **2017**, *10*, 2782–2799. [[CrossRef](#)]
47. Komori, Y.; Sugahara, Y. A kaolinite-NMF-methanol intercalation compound as a versatile intermediate for further intercalation reaction of kaolinite. *J. Mater. Res.* **1998**, *13*, 930–934. [[CrossRef](#)]
48. Komori, Y.; Sugahara, Y.; Kuroda, K. Intercalation of alkylamines and water into kaolinite with methanol kaolinite as an intermediate. *Appl. Clay Sci.* **1999**, *15*, 241–252. [[CrossRef](#)]
49. Matusik, J.; Kłapyta, Z. Characterization of kaolinite intercalation compounds with benzylalkylammonium chlorides using XRD; TGADTA and CHNS elemental analysis. *Appl. Clay Sci.* **2013**, *83–84*, 433–440. [[CrossRef](#)]
50. Matusik, J.; Kłapyta, Z.; Olejniczak, Z. NMR and IR study of kaolinite intercalation compounds with benzylalkylammonium chlorides. *Appl. Clay Sci.* **2013**, *83–84*, 426–432. [[CrossRef](#)]
51. Gardolinski, J.E.F.C.; Lagaly, G. Grafted organic derivatives of kaolinite: I. Synthesis; chemical and rheological characterization. *Clay Miner.* **2005**, *40*, 537–546. [[CrossRef](#)]
52. Gardolinski, J.E.F.C.; Lagaly, G. Grafted organic derivatives of kaolinite: II. Intercalation of primary n-alkylamines and delamination. *Clay Miner.* **2005**, *40*, 547–556. [[CrossRef](#)]
53. Liu, Q.F.; Li, X.; Cheng, H.F. Insight into the self-adaptive deformation of kaolinite layers into nanoscrolls. *Appl. Clay Sci.* **2016**, *124–125*, 175–182. [[CrossRef](#)]
54. Sidheswaran, P.; Bhat, A.N.; Ganguli, P. Intercalation of salts of fatty acids into kaolinite. *Clays Clay Miner.* **1990**, *38*, 29–32. [[CrossRef](#)]
55. Wang, S.; Zuo, X.; Cheng, H.F.; Yang, Y.; Liu, Q.F. Structural model and de-intercalation kinetics of kaolinite-methanol-sodium stearate intercalation compound. *J. Braz. Chem. Soc.* **2016**, *27*, 1311–1318. [[CrossRef](#)]
56. Li, X.G.; Cui, X.J.; Wang, S.; Wang, D.; Li, K.; Liu, Q.F.; Komarneni, S. Methoxy-grafted kaolinite preparation by intercalation of methanol: Mechanism of its structural variability. *Appl. Clay Sci.* **2017**, *137*, 241–248. [[CrossRef](#)]
57. Horváth, E.; Kristóf, J.; Frost, R.L. Vibrational spectroscopy of intercalated kaolinites. Part I. *Appl. Spectrosc. Rev.* **2010**, *45*, 130–147. [[CrossRef](#)]
58. Dong, W.J.; Li, W.J.; Yu, K.F.; Krishna, K.; Song, L.Z.; Wang, X.F.; Wang, Z.C.; Marc-Oliver, C.; Feng, S.H. Synthesis of silica nanotubes from kaolin clay. *Chem. Commun.* **2003**, *11*, 1302–1303. [[CrossRef](#)]
59. Liu, Q.F.; Wang, D.; Guo, P.; Zhang, S.L.; Cheng, H.F.; Li, X.G.; Zhang, S. Preparation and structural characterization of kaolinite intercalation compound with Series of quaternary ammonium salt. *J. Chin. Ceram. Soc.* **2015**, *2*, 222–230.
60. Yuan, P.; Tan, D.Y.; Annabi-Bergaya, F.; Yan, W.C.; Liu, D.; Liu, Z.W. From platy kaolinite to aluminosilicate nanoroll via one-step delamination of kaolinite: Effect of the temperature of intercalation. *Appl. Clay Sci.* **2013**, *83–84*, 68–76. [[CrossRef](#)]

